Quantification of Brain Glucose Metabolism by ^{18}F-FDG PET with Real-Time Arterial and Image-Derived Input Function in Mice

Malte F. Alf[1,2], Matthias T. Wyss[3,4], Alfred Buck[3], Bruno Weber[4], Roger Schibli[1,5], and Stefanie D. Krämer[1]

[1]Center for Radiopharmaceutical Sciences of ETH, PSI, and USZ, Institute of Pharmaceutical Sciences, Department of Chemistry and Applied Biosciences, ETH Zurich, Zurich, Switzerland; [2]Laboratory of Functional and Metabolic Imaging, Institute of Physics of Biological Systems, Ecole Polytechnique Fédérale de Lausanne, Lausanne, Switzerland; [3]Department of Nuclear Medicine, University Hospital Zurich, Zurich, Switzerland; [4]Institute of Pharmacology and Toxicology, University of Zurich, Zurich, Switzerland; and [5]Center for Radiopharmaceutical Sciences of ETH, PSI, and USZ, Paul Scherrer Institute PSI, Villigen, Switzerland

Kinetic modeling of PET data derived from mouse models remains hampered by the technical inaccessibility of an accurate input function (IF). In this work, we tested the feasibility of IF measurement with an arteriovenous shunt and a coincidence counter in mice and compared the method with an image-derived IF (IDIF) obtained by ensemble-learning independent component analysis of the heart region. **Methods:** ^{18}F-FDG brain kinetics were quantified in 2 mouse strains, CD1 and C57BL/6, using the standard 2-tissue-compartment model. Fits obtained with the 2 IFs were compared regarding their goodness of fit as assessed by the residuals, fit parameter SD, and Bland–Altman analysis. **Results:** On average, cerebral glucose metabolic rate was 10% higher for IDIF-based quantification. The precision of model parameter fitting was significantly higher using the shunt-based IF, rendering the quantification of single process rate constants feasible. **Conclusion:** We demonstrated that the arterial IF can be measured in mice with a femoral arteriovenous shunt. This technique resulted in higher precision for kinetic modeling parameters than did use of the IDIF. However, for longitudinal or high-throughput studies, the use of a minimally invasive IDIF based on ensemble-learning independent component analysis represents a suitable alternative.

Key Words: energy metabolism; PET; molecular imaging; glucose; kinetic modeling

J Nucl Med 2013; 54:132–138
DOI: 10.2967/jnumed.112.107474

PET with ^{18}F-FDG is a commonly used method to determine glucose metabolism in animal and human tissues (*1*). Full quantification of ^{18}F-FDG kinetics can be achieved by applying a 2-tissue-compartment model (*2*). The model requires the time course of the ^{18}F-FDG concentration in the target organ (tissue time–activity curve) and in arterial plasma (input function, IF). In human brain PET, the IF is commonly measured from a catheter placed in the radial artery. An alternative is derivation of the IF from PET images via values measured in a volume of interest placed over the cardiac ventricles or a large vessel. A prerequisite of image-derived IFs (IDIFs) is the location of the blood pool and the organ of interest in the same field of view. In general, one or more arterial blood samples are measured to calibrate the IDIF. In a recent review article for human PET (*3*), the authors concluded that arterial blood sampling remains the preferred method to define the IF, because invasiveness is hardly reduced by the use of an IDIF.

In small animals, the small blood volume is the major constraint for manual blood sampling. This constraint prompted the development of several alternative methods, such as the sampling of very small volumes via a microfluidic chip (*4*) or the use of β-probes for measuring the blood radioactivity (*5,6*). Despite these new physical methods, the main research focus has been on developing the use of IDIFs, where blood radioactivity is estimated directly from the dynamic PET images. IDIF generation from simple analysis of blood pool volumes such as the liver or the heart ventricles is flawed by ^{18}F-FDG uptake by the liver or spillover from surrounding myocardium, cardiac motion, and partial-volume effects. Compensation can be achieved to varying degrees by image processing methods such as factor analysis (*7*), model-based techniques (*8*), independent component analysis (*9*), so-called hybrid IDIFs (e.g., *10,11*), and cardiac gating combined with improved image reconstruction algorithms (*12*). Most of these methods rely on at least 1 measure from a blood sample for scaling of the IDIF. Hence, blood sampling is not entirely obviated.

Received Apr. 14, 2012; revision accepted Jul. 27, 2012.
For correspondence or reprints contact either of the following:
Stefanie Krämer, Center for Radiopharmaceutical Sciences of ETH, PSI, and USZ, Institute of Pharmaceutical Sciences, Department of Chemistry and Applied Biosciences, ETH Zurich, Wolfgang-Pauli-Strasse 10, CH-8093 Zurich, Switzerland.
E-mail: stefanie.kraemer@pharma.ethz.ch
Roger Schibli, Center for Radiopharmaceutical Sciences of ETH, PSI, and USZ, Institute of Pharmaceutical Sciences, Department of Chemistry and Applied Biosciences, ETH Zurich, Wolfgang-Pauli-Strasse 10, CH-8093 Zurich, Switzerland.
E-mail: roger.schibli@pharma.ethz.ch
Published online Nov. 15, 2012.

To our knowledge, there is currently no gold standard to define the real-time ^{18}F-FDG arterial IF in mice in a reliable and easily accessible manner. In this study, we adapted a method for direct blood radioactivity measurements and an approach for the generation of IDIFs for use in mice. We acquired real-time blood radioactivity curves by means of a new coincidence counter in combination with an arteriovenous shunt and compared the findings to IDIFs generated from PET data of the cardiac region with an ensemble-learning independent component analysis (EL-ICA) algorithm (*13*). We used 2 different mouse strains to explore the possible strain dependency of our methods: C57BL/6 mice, because they are relevant for studies of genetically modified animals, and CD1 mice, because they are valuable as disease models, such as cerebral ischemia (*14*). The purpose of this work was 2-fold. First, we evaluated whether the arteriovenous-shunt/counter technique, which was previously demonstrated in rats (*15*), is also feasible in mice. Second, we compared ^{18}F-FDG kinetic parameters and fit precisions obtained with the experimental shunt IF and the IDIF.

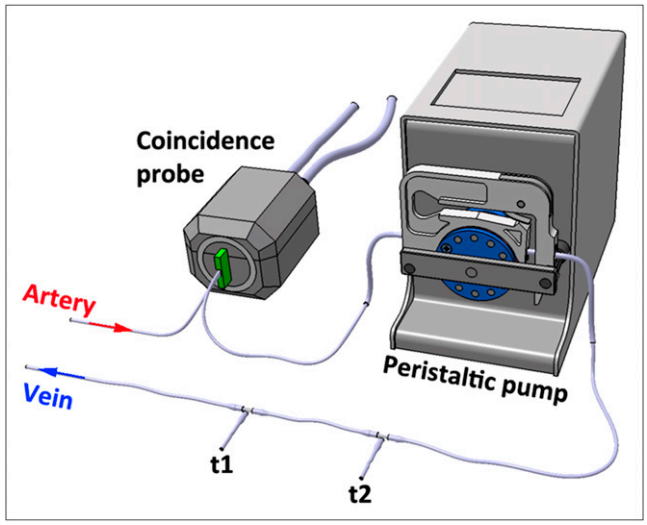

FIGURE 1. Schematic of arteriovenous shunt setup. Blood, driven by peristaltic pump, flows from femoral artery through coincidence probe and back to femoral vein. Two 3-way valves, t1 and t2, are used for tracer application and blood sampling, respectively.

MATERIALS AND METHODS

Animal Preparation

All animal experiments were performed by licensed investigators, and the experimental procedures were reviewed by an ethical committee and authorized by the veterinary authority of the canton Zurich. Methods conformed to the guidelines of the Swiss Animal Protection Law (Act of Animal Protection, December 16, 2005, and Animal Protection Ordinances, April 23, 2008, and April 12, 2010). Male CD1 mice ($n = 10$; weight, 37.2 ± 2.6 g) and male C57BL/6 mice ($n = 5$; 26.1 ± 1.4 g) were obtained from Charles River. The mice were housed under approved conditions with no special husbandry and had free access to food and water before the experiments.

For surgery, the animals were anesthetized with isoflurane at approximately a 2% maintenance dose in a 2:1 mixture of air and oxygen. Body temperature was maintained at 37°C by means of a heating pad (Harvard Apparatus). Polyethylene catheters (PE10 with an internal diameter of 0.28 mm; Smiths Medical) filled with heparinized (20 IU/mL) saline were inserted into the right femoral artery and vein with the help of a stereomicroscope and securely fastened with ligatures (6-0 silk thread). Additionally, catheters were held in place with tape. The animals were kept under anesthesia for all subsequent procedures.

Data Acquisition

After the animal had been placed on the PET/CT scanner (VISTA eXplore [GE Healthcare]; axial FOV of 4.8 cm), a CT scout image was acquired and the bed position was adjusted for the subsequent PET scan to include the heart and the brain in the FOV. The arterial and venous catheters were connected to an arteriovenous shunt running through a coincidence counter (twilite; Swisstrace GmbH) positioned next to the scanner bed. The volume inside the counter was approximately 6 μL (10 cm of PE10). The arteriovenous shunt was also used for radiotracer injection (Fig. 1). The total volume of the tube system was approximately 60 μL. Counter data were recorded with the acquisition tool of the imaging software, PMOD, version 3.3 (PMOD Technologies Inc.). A constant flow of 120 μL/min was maintained by a peristaltic pump (Ismatec; Wertheim-Mondfeld). This corresponds to about half the average velocity we, as well as Yu et al. (*16*), observed in a short piece of PE10 tube driven by the animal's blood pressure and was chosen because it can be expected not to influence the overall and thus brain physiology within a normal blood pressure range.

For PET acquisition, the respiration rate was monitored (1025 L; SA Instruments) and maintained at 90 bpm by adjusting the isoflurane dose if required. Body temperature was kept at 37°C by a fan controlled by a rectal temperature probe. A dynamic list-mode PET scan (45 min), recording of the blood coincidence counter, and infusion of ^{18}F-FDG (routine production for clinical use; University Hospital Zurich) were started simultaneously. ^{18}F-FDG was infused in 100–150 μL of saline over a period of 4–6 min with a syringe pump (Harvard Apparatus). Injected activities were between 10 and 16 MBq. Immediately after the PET acquisition, an arterial blood sample was collected in a heparinized vial, and plasma was separated by centrifugation. Plasma glucose was measured with a glucose oxidase/reflectance system (Vitros DT60 II; Ortho Clinical Diagnostics). Meanwhile, a CT scan was acquired for anatomic orientation. The anesthetized animals were then sacrificed by decapitation.

The coincidence counter and PET scanner were calibrated to kBq/cm^3 once per day by means of a phantom scan: A 5-mL syringe and a piece of PE10 tube were filled with the same ^{18}F-FDG solution of known radioactivity concentration (~1 MBq/mL), mimicking the conditions of a PET mouse scan. A static scan of 5 min was acquired in parallel with a coincidence counter measurement of the PE10 tube.

Image Analysis

PET images were reconstructed to a nominal voxel size of 0.3875 × 0.3875 × 0.775 mm (actual resolution of 0.9 mm in full width at half maximum in the center of the FOV (*17*)) with a 3-dimensional FORE/2-dimensional OSEM algorithm and user-defined time frames. Scatter correction was applied. Data were not corrected for attenuation, as suggested for mice by our recent system evaluation (*17*). The shortest frames had a duration of 10 s and were grouped around the time when infusion was stopped, that is, when plasma ^{18}F-FDG concentration changed most rapidly.

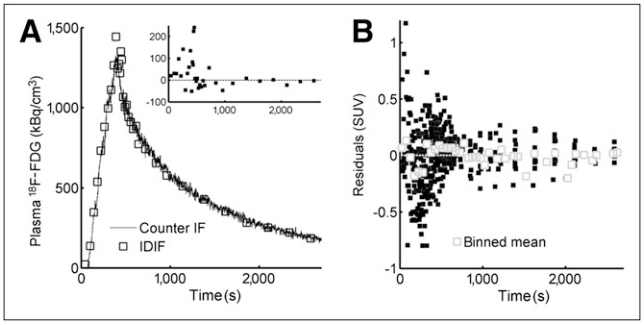

FIGURE 2. (A) Representative shunt IF and corresponding IDIF. Squares represent averaged radioactivity of each time frame at respective mid time frame. (Inset) Differences (IDIF − shunt IF). Deviations are mostly in short frames around peak where infusion stops. (B) Differences as in A from all scanned mice and their binned means, normalized by injected dose per gram of body weight (standardized uptake value [SUV]). Mean of residuals is not systematically different from zero ($P > 0.38$); their temporal average is 0.009 ± 0.227.

The maximum frame lengths toward the end of the scan were 4 min (Fig. 2). The software package PMOD (PMOD Technologies Ltd.) was used for PET data analysis and kinetic modeling. For each mouse, a brain volume of interest was defined manually corresponding to the cerebrum, guided by the coregistered CT scan (Supplemental Fig. 1; supplemental materials are available online only at http://jnm.snmjournals.org). The brain time–activity curve was generated from this volume of interest and converted to kBq/cm^3.

Shunt/Coincidence Counter IF

The whole-blood radioactivity measurements from the coincidence counter were corrected for counter crystal background counts. Background counts were about 125 cps, that is, 18%–25% of the maximum value around the infusion stop and 25%–70% of the total value at 45 min. The remaining coincidence counts were then corrected for ^{18}F decay before conversion to plasma radioactivity by applying a correction for erythrocyte uptake, given by Equation 1 (*16*),

$$A_{plasma} = A_{whole\ blood} \times \left(0.39 \times e^{-0.19t} + 1.17\right), \qquad \text{Eq. 1}$$

where A_{plasma} and $A_{whole\ blood}$ are the radioactivity in plasma and whole blood, respectively, at time t in minutes after the start of ^{18}F-FDG infusion. To reduce statistical noise caused by the random nature of radioactive decay, a moving average over 5 s was used to smooth the IF. The experimentally determined dispersion of a 5-s step function in the coincidence counter tube was used to evaluate the influence of dispersion on the experimental IF. The simulated effect was negligible (Supplemental Fig. 2).

IDIF

A cuboid volume of interest was defined around the whole heart of each animal. A representative transversal cross-section is shown in Figure 3. PET image data within the volume of interest were transformed to a matrix with the format voxel × time frame with MATLAB (The MathWorks Inc.). The data matrix was processed by EL-ICA. The algorithm was developed by Naganawa et al. for human brain PET (*13*). The original EL-ICA framework was created at Cambridge University (*18*). We adjusted the set of initial options to match the convergence criteria and the initially assumed noise variance to our data. A rectified gaussian and a Laplacian-shaped distribution were used as priors for the mixing matrix and source image, respectively.

All time frames of the reconstructed PET data were included in the analysis. Analogous to the analysis by Naganawa et al. (*13*), we assumed 2 components to be estimated by the EL-ICA, representing the radioactivity in the blood and tissue compartments, respectively. The resulting time curve corresponding to the blood component was scaled with two 20-s averages from the decay-corrected coincidence counter data, one at roughly 1,000 s and the other at the middle of the last frame at 2,600 s. Scaling included multiplication by a factor and addition of a constant. The scaled curves were then translated to plasma radioactivity, that is, to the IDIF, as described in Equation 1.

Kinetic Modeling

The standard ^{18}F-FDG 2-tissue-compartment model (*2*) was fitted to the brain time–activity curve, with either the IDIF or the shunt IF. For the latter, a delay corresponding to the transfer time of blood (approximately 10 s) from the femoral artery to the counter was included in the model. Fitting was performed using the Levenberg–Marquardt algorithm. A blood fraction of 5.5% was assumed for the brain time–activity curve, as indicated by recent micro-CT findings in mice (*19*). The 2-tissue-compartment model is defined by the following rate constants: K_1 (apparent influx rate constant), k_2 (efflux rate constant), k_3 (phosphorylation rate constant), and k_4 (rate constant of dephosphorylation). The hybrid ^{18}F-FDG uptake constant (K_{FDG}) and cerebral glucose metabolic rate (CMR_{glc}) were calculated as shown in Equations 2 and 3, respectively:

$$K_{FDG} = \frac{K_1 \times k_3}{k_2 + k_3} \qquad \text{Eq. 2}$$

$$CMR_{glc} = \frac{K_{FDG} \times C_p}{LC}, \qquad \text{Eq. 3}$$

where C_p denotes the glucose concentration in plasma and LC the lumped constant. The lumped constant was set to 0.6 to allow for direct comparison of our results with those of Yu et al. (*16*). For

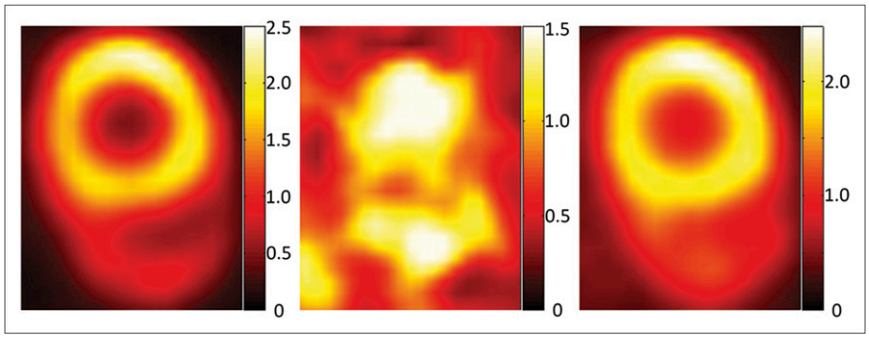

FIGURE 3. Source images corresponding to independent components used to generate IDIF: tissue component (left), blood component (middle), and original PET image (right). Image borders correspond to boundaries of heart volume of interest in respective dimensions. Color axis is in arbitrary units (EL-ICA is not scale-invariant).

comparison, CMR_{glc} was estimated from Patlak plots including the data from 15 to 45 min after injection for linear regression.

Statistical Analysis

To compare the 2 methods, that is, ^{18}F-FDG kinetic modeling with the shunt IF and the IDIF, correlations were calculated for estimates of K_{FDG} and CMR_{glc}, respectively, each estimated with either IF type. Bland–Altman plots (*20*) were generated to further visualize the comparison. Correlations of the single rate constants K_1–k_4 as estimated with either IF type were calculated. The SDs of the fit of individual rate constants with either counter IF or IDIF were compared with F tests, and the results were corrected for multiple comparisons with the Bonferroni adjustment. Fit parameters of the 2 mouse strains were compared with 2-tailed homoscedastic *t* tests. Data are presented as mean ± SD.

RESULTS

Plasma glucose levels ranged from normal to high glycemic values in C57BL/6 mice (11.8 ± 4.1 mmol/L; range, 6.7–16.9 mmol/L; $n = 5$), whereas CD1 mice showed a wider range (8.5 ± 5.4; range, 1.9–19.2 mmol/L; $n = 10$). Excluding 2 CD1 mice with extreme values, plasma glucose levels reached 5.4–13.0 mmol/L in the CD1 mice ($n = 8$).

IFs

For all animals, the source images corresponding to the estimated independent components separated the lumina of the ventricles, that is, the blood pool, from the myocardium, that is, the tissue compartment. Figure 3 shows an example of a representative set of images. IDIFs were generated from the EL-ICA results as described above. Agreement with the respective real-time shunt IF was good (Fig. 2); all R^2 obtained with linear correlation of the 2 IFs were greater than 0.89, suggesting no major differences in shape. Differences were present mostly around the peak at the end of the infusion, when PET frame lengths were shortest. For comparison, residuals were normalized to injected dose per gram of body weight. The mean of the residuals of all datasets was not significantly different from zero (0.0087 ± 0.227, $P > 0.38$; Fig. 2B). The IFs are shown with a logarithmic time scale in Supplemental Figure 3. A comparison of the individual shunt IFs revealed large differences and a dependency of their shape on plasma glucose levels, therefore prohibiting the use of a population standard IF.

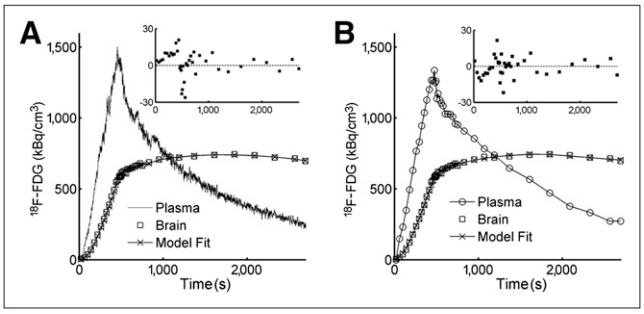

FIGURE 4. Kinetic model fits of CD1 mouse brain time–activity curve with respective IFs. (A) Model fit applying shunt IF (R^2 = 0.999). (B) Model fit of same time–activity curve with corresponding IDIF (R^2 = 0.998). Insets show residual differences between model fit and brain time–activity curve.

Compartment Modeling of ^{18}F-FDG Uptake in the Brain

Brain (cerebrum) PET data were fitted with the ^{18}F-FDG 2-tissue-compartment model with both IDIFs and shunt IFs (Fig. 4). A typical PET/CT image is shown in Supplemental Figure 1. Excellent fits were obtained in all animals with both IFs (all $R^2 > 0.99$ for both mouse strains and types of IF). The 2 fits of a representative dataset are shown in Figure 4. Of the 10 CD1 mice, the 2 animals with the lowest and highest plasma glucose concentrations were excluded from the following statistical tests because the fit with the IDIF did not converge to a solution with physiologic K_1 and k_2.

The mean value for the K_{FDG} achieved with the shunt IF was 0.035 ± 0.013 mL/cm^3/min and 61 ± 11 μmol/min/100 g for CMR_{glc} in C57BL/6 mice, which is higher than the 40.6 ± 13.3 μmol/min/100 g in the cerebral cortex published previously by Yu et al. (*16*). The respective values in CD1 mice were higher (0.057 ± 0.019 mL/cm^3/min and 75 ± 24 μmol/min/100 g, $n = 8$), but the differences between strains were not statistically significant ($P > 0.05$ and $P > 0.25$). Table 1 provides an overview of the rate constants and metabolic rates. Good correlations were obtained for K_{FDG} and CMR_{glc}, respectively, comparing their estimations with the IDIF and shunt IF (Fig. 5). Plotting K_{FDG} values from the fits with shunt IF versus IDIF resulted in a slope of 0.932, indicating a tendency toward estimating higher values when IDIFs are used (Fig. 5A). The slope was 0.902 for CMR_{glc} (Fig. 5B). This discrepancy between the 2 methods is also reflected by the Bland–Altman plots in Figures 5C (K_{FDG}) and 5D (CMR_{glc}).

Rate constants K_1, k_2, and k_3 were higher by trend for the IDIF. Correlations comparing the single process rate constants applying IDIF and shunt IF were moderate for K_1 ($K_{1,shunt} = 0.31 \times K_{1,IDIF} + 0.17$, $R^2 = 0.47$, and $K_{1,shunt} = 0.57 \times K_{1,IDIF} + 0.08$, $R^2 = 0.38$, for CD1 and C57BL/6, respectively) and significant only for CD1 mice ($P < 0.05$), for which n was higher (8 vs. 5). No significant correlation was found for k_2 in either strain. Correlations significantly different from zero were found for k_3 ($k_{3,shunt} = 0.38 \times k_{3,IDIF} + 0.08$, $R^2 = 0.65$, and $k_{3,shunt} = 1.33 \times k_{3,IDIF} + 0.07$, $R^2 = 0.94$, for the 2 strains) and k_4 ($k_{4,shunt} = 0.52 \times k_{4,IDIF} + 0.02$, $R^2 = 0.65$, and $k_{4,shunt} = 0.89 \times k_{4,IDIF} + 0.003$, $R^2 = 0.69$, respectively), with $P < 0.05$ for CD1 but not C57BL/6.

Patlak Analysis

Graphical analysis yielded CMR_{glc} values of 38 ± 10 and 39 ± 17 μmol/min/100 g in C57BL/6 mice with the

TABLE 1
Average Rate Constants and Metabolic Rates

Strain	Method	K_1 (mL/min/cm^3)	k_2 (1/min)	k_3 (1/min)	k_4 (1/min)	K_{FDG} (mL/min/cm^3)	CMR_{glc} (μmol/min/100 g)
CD1 (n = 8)	Shunt	0.25 ± 0.04	0.48 ± 0.16	0.13 ± 0.03	0.03 ± 0.015	0.057 ± 0.019	75 ± 24
	IDIF	0.30 ± 0.11	0.55 ± 0.25	0.23 ± 0.14	0.03 ± 0.018	0.063 ± 0.03	79 ± 30
C57BL/6 (n = 5)	Shunt	0.27 ± 0.09	0.57 ± 0.10	0.08 ± 0.02	0.018 ± 0.004	0.035 ± 0.013	61 ± 11
	IDIF	0.33 ± 0.10	0.81 ± 0.09	0.11 ± 0.02	0.025 ± 0.004	0.041 ± 0.013	73 ± 20

Values are mean ± SD.

shunt IF and IDIF, respectively, and 43 ± 20 vs. 42 ± 18 μmol/min/100 g in CD1 mice. These values were significantly (both $P < 0.05$) lower than those obtained by the 2-tissue-compartment model for both strains. No significant differences were found between the fit precision obtained with either IF type.

Influence of the Type of IF on the Goodness of Fit

To evaluate the influence of the type of IF on the goodness of fit of the 2-compartment model, the relative SDs of the single fit parameters as revealed by PMOD with the Levenberg–Marquardt algorithm were compared via F tests (Table 2). The use of the shunt IF resulted in significantly more precise (smaller SD) fits of K_1 and k_2 in all animals, as well as of k_3 in most and k_4 in some animals. The alternative hypothesis ($\sigma^2_{\text{shunt IF}} > \sigma^2_{\text{IDIF}}$) had no significant results for any rate constant in any dataset. The model fit residuals (χ^2) were not markedly different for the 2 methods. F tests, corrected for multiple comparisons, showed a significantly ($P < 0.001$) smaller fit SD for K_{FDG} and CMR_{glc} when the shunt IF was used in all C57BL/6 mice and 5 of the 8 CD1 mice.

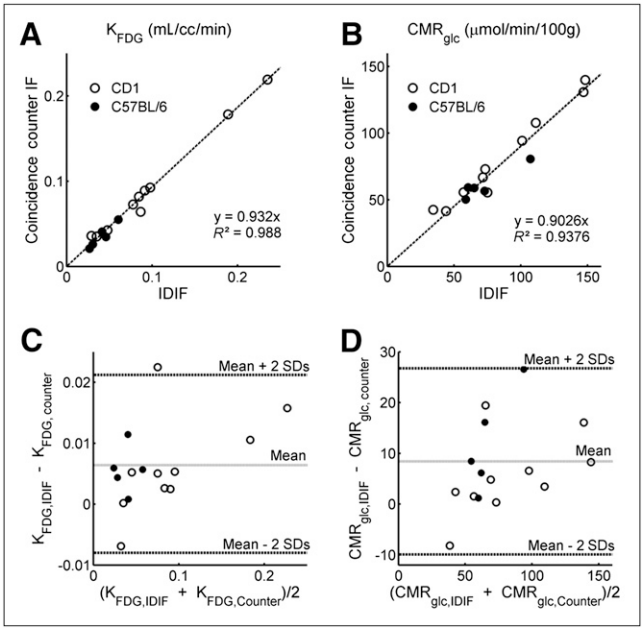

FIGURE 5. Correlations and Bland–Altmann plots for K_{FDG} and CMR_{glc} determined with shunt IF and IDIF. (A) K_{FDG} and (B) CMR_{glc} estimates achieved with either type of IF show almost perfect linear correlation. (C) and (D) Bland–Altmann plots for K_{FDG} and CMR_{glc} indicating higher values when determined with IDIF and relatively large interval of ±2 SDs, suggesting that at least 1 method is of mediocre reliability.

DISCUSSION

In this work, we demonstrated that the measurement of the input curve with a coincidence counter in mice is feasible with practically real-time resolution and no blood loss. The measurement of the blood time–radioactivity curve with the shunt/coincidence counter system resulted in a high precision of the kinetic model fit.

The question arises as to the gold standard with which to compare our measurements. In general, the gold standard would be manual blood sampling. However, it is not possible to obtain a time-resolved IF by manual sampling in mice because of the small overall blood volume. We believe that the measurement in the shunt has no disadvantages compared with manual sampling and provides a suitable alternative standard. This was demonstrated in rats, where manual sampling and shunt measurements yielded practically identical results (*15*). The shunt features additional relevant benefits such as minimal blood loss, real-time temporal input curve resolution, and a practical means for infusion of tracer and pharmacologic agents. It provides high signal linearity and reliability and is independent of surrounding electromagnetic fields, in contrast to β-probe systems (*6,21*), which constitute the only alternative approach currently available with a similar temporal resolution yielding full input curves. The β-probe approach depends heavily on the positioning of the detector and suffers from a lower sensitivity.

The model values obtained using the IDIF are higher by a 7% and 10% mean difference for K_{FDG} and CMR_{glc}, respectively, with a relatively high variability in the mean differences, as seen in the Bland–Altman plots. The nonsystematic deviations could result from the differences in height and temporal distribution of the residuals comparing the 2 types of IF around the peak period. Another likely explanation is the lower temporal resolution of the IDIF and an associated overfitting. Despite these average differences, the estimations correlated strongly between the 2 methods used. This is in line with previous publications reporting decent agreement even for input curves with highly incon-

TABLE 2
Fitting Precision with 2 Types of IF

Parameter	K_1 (mL/min/cm^3)	SD (%)	k_2 (1/min)	SD (%)	k_3 (1/min)	SD (%)	k_4 (1/min)	SD (%)	K_{FDG} (mL/min/cm^3)	SD (%)
IDIF 1	0.296	10.383	0.766	17.056	0.125	11.805	0.024	13.232	0.041	5.837
IDIF 2	0.269	6.967	0.907	10.766	0.101	9.582	0.029	11.626	0.027	5.749
IDIF 3	0.238	7.291	0.731	12.545	0.107	12.106	0.023	17.610	0.031	6.845
IDIF 4	0.468	6.746	0.920	10.273	0.101	8.988	0.019	17.181	0.046	5.454
IDIF 5	0.402	5.726	0.736	9.455	0.131	6.717	0.027	6.876	0.061	3.297
Shunt 1	0.294	1.450	0.653	2.013	0.105	3.497	0.022	7.980	0.041	2.449
Shunt 2	0.162	1.245	0.430	1.937	0.064	4.854	0.020	11.587	0.021	3.311
Shunt 3	0.226	1.016	0.614	1.405	0.080	3.515	0.017	9.384	0.026	2.515
Shunt 4	0.284	0.573	0.482	0.799	0.067	1.838	0.012	8.476	0.035	1.379
Shunt 5	0.407	1.072	0.656	0.945	0.102	2.397	0.022	4.354	0.055	1.331
$\sigma^2_{IDIF} > \sigma^2_{shunt}$	df	*F*		*F*		*F*		*F*		*F*
Mouse 1	26/26	52.041*		98.696*		16.142*		3.517		5.918*
Mouse 2	29/29	86.185*		137.309*		9.716*		2.136		4.975*
Mouse 3	27/27	57.444*		112.981*		21.159*		6.656*		10.104*
Mouse 4	29/29	377.026*		603.740*		53.824*		9.845*		27.648*
Mouse 5	30/30	27.875*		125.813*		12.774*		3.767		7.475*

Original data from C57BL/6 mice used in this study. *F* tests revealed significantly (*$P < 0.01$, corrected for multiple comparisons, with df depending on number of image frames in respective PET dataset) larger variances in fitted parameters using IDIF than using shunt IF. Pattern was similar in CD1 mice, for which K_1 and k_2 could be estimated with significantly ($P < 0.01$) higher precision in all animals, and k_3, k_4, and K_{FDG} in 6, 3, and 4 of 8 animals, respectively.

gruous shapes (e.g., *16,22*). IDIFs are, therefore, a valid alternative for the estimation of CMR_{glc}, in particular in cases where a shunt surgery is not possible, for example, in longitudinal studies.

In general, 2-tissue-compartment modeling of K_{FDG} and CMR_{glc} based on the shunt IF yielded smaller SDs, most probably because of the higher sampling rate and greater precision in the rate constants achieved with the shunt and counter. This interpretation is supported by the lack of difference in the CMR_{glc} estimated with either IF type by Patlak analysis, which is less sensitive to the shape of the IF than the 2-tissue-compartment model.

Several methods exist to compute IDIFs. The EL-ICA algorithm was chosen because it uses a high amount of information present in the image data and features a nonnegativity constraint that prevents physically meaningless results and makes the method more robust (*13*). The use of EL-ICA allowed us to filter out spillover of the myocardium and partial-volume effects. We further optimized the data quality by applying a relatively slow infusion protocol for ^{18}F-FDG to avoid the unphysiologic mixing conditions in the blood and the corresponding overshoot in plasma radioactivity that occur after bolus injection. Furthermore, we included the fractional cerebral blood volume into the kinetic model, a correction that was not done by Yu et al. (*16*). The combination of the above precautions resulted in model fits with high R^2 values and meaningful estimates of the single rate constants.

With both IF methods, we found a significant contribution of ^{18}F-FDG-6-phosphate dephosphorylation to the kinetics. This contribution was indicated by k_4, which is not negligible in the fits, in good agreement with the observations by Yu et al. (*16*). For this reason, we did not further develop the results obtained by Patlak analysis since it assumes irreversible phosphorylation. Dephosphorylation, which is considered by k_4 in the 2-tissue-compartment model, results in an underestimation of CMR_{glc} in the Patlak analysis, as observed in our study and that by Yu et al. (*16*). The results of our Patlak analysis were higher ($P < 0.05$) by a factor of about 2 than those of Wong et al. (*23*). Possible influencing factors that may have differed between the 2 studies include the duration of anesthesia, which in our study included the time for the surgery; the depth of anesthesia; and the oxygen content of the inhaled gas mix. Isoflurane anesthesia increases plasma glucose and with it CMR_{glc}, as demonstrated by Saha et al. (*24*). The authors showed an increase in blood glucose levels in nonfasted rats during an experimental period of 180 min of isoflurane anesthesia (2.5%). The increase was highest within the first 60 min. In our experiments, the PET scan started 45–60 min after the induction of anesthesia, and isoflurane doses were lower (~2%). We therefore assume that the plasma glucose concentrations measured after the scan are representative of the complete scan duration in our study. Finally, this may explain why our values are higher than those reported by Yu et al. (*16*), who measured plasma glucose before the scan. Intersubject variability in plasma glucose concentration and hence the shape of the IF may hamper the use of population-based standard IFs in mice, for which it is currently impossible to reliably clamp plasma glucose to a standard normoglycemic value.

A drawback of our IDIF and most other image-derived methods previously proposed is the need for scaling with blood

samples. In our case, because of the Bayesian nature of the IDIF-generating algorithm, at least 2 samples were required for correct scaling. Furthermore, to achieve an accurate scaling, the 2 samples have to be temporally separated by at least several minutes and ideally have a significantly different activity concentration. Also, at least at time points before steady state is reached, arterial samples are clearly preferable.

No positive correlation was found between the efflux rate constants k_2 based on the IDIF and the shunt IF model fits. This is not surprising considering the high relative SD of k_2 in the fits with the IDIFs. Compared with the shunt IF, the IDIF is poorly defined around its maximum where plasma ^{18}F-FDG concentration changes most. Although the shunt method allows for sufficient temporal resolution in this region, the IDIF suffers from a compromise between duration of time frames and counting precision. The efflux rate constant k_2 affects the early time points of the tissue time–activity curve and is, therefore, more sensitive to this early part of the IF while k_3 and k_4 are more dependent on later time points. This emphasizes the necessity for IFs with adequate time resolution and accurate counting precision for the determination of the single process rate constants. Both conditions are met with the shunt method.

CONCLUSION

We showed that the IF can be measured with high temporal resolution in mice using a femoral arteriovenous shunt. The single process rate constants K_1–k_4 can be determined with higher precision with the shunt/counter IF than with the IDIF. The shunt method represents a step forward toward more conclusive, quantitative analysis of PET studies in mouse models of, for example, glucose transporter deficiency or mutant and knock-out variants of other proteins relevant for energy metabolism. It also opens new avenues for investigations of disease models of diabetes and possibly ischemic stroke. Quantification of ^{18}F-FDG kinetics in mouse brain PET using an IDIF leads to a less precise estimation of individual parameters and, therefore, values for glucose consumption than the shunt method. However, keeping its limitations in mind, the use of an IDIF-based method on EL-ICA represents an appropriate alternative for longitudinal or high-throughput studies, when the invasive measurement of blood activity is not feasible.

DISCLOSURE

The costs of publication of this article were defrayed in part by the payment of page charges. Therefore, and solely to indicate this fact, this article is hereby marked "advertisement" in accordance with 18 USC section 1734. This work was supported in part by the Swiss National Competence Center for Biomedical Imaging (NCCBI) and by the Swiss National Foundation (PP00B-110751/1 and 31003A-124739/1). Two of the authors developed the blood sampling system used in this work and are cofounders of Swisstrace GmbH. No other potential conflict of interest relevant to this article was reported.

ACKNOWLEDGMENTS

We are grateful to Dr. Mika Naganawa, who kindly provided MATLAB-code for this study. We thank Claudia Keller and Petra Wirth for technical assistance and Stefan Weber for the graphics rendering of the shunt setup.

REFERENCES

1. Bailey DL, Townsend DW, Valk PE, Maisey MN, eds. *Positron Emission Tomography: Basic Sciences*. London, U.K.: Springer; 2005:1–2.
2. Sokoloff L, Reivich M, Kennedy C, et al. The [^{14}C]deoxyglucose method for the measurement of local cerebral glucose utilization: theory, procedure, and normal values in the conscious and anesthetized albino rat. *J Neurochem.* 1977;28:897–916.
3. Zanotti-Fregonara P, Chen K, Liow JS, Fujita M, Innis RB. Image-derived input function for brain PET studies: many challenges and few opportunities. *J Cereb Blood Flow Metab.* 2011;31:1986–1998.
4. Wu HM, Sui G, Lee CC, et al. In vivo quantitation of glucose metabolism in mice using small-animal PET and a microfluidic device. *J Nucl Med.* 2007;48:837–845.
5. Laforest R, Sharp TL, Engelbach JA, et al. Measurement of input functions in rodents: challenges and solutions. *Nucl Med Biol.* 2005;32:679–685.
6. Convert L, Morin-Brassard G, Cadorette J, Archambault M, Bentourkia M, Lecomte R. A new tool for molecular imaging: the microvolumetric beta blood counter. *J Nucl Med.* 2007;48:1197–1206.
7. Wu HM, Hoh CK, Choi Y, et al. Factor analysis for extraction of blood time-activity curves in dynamic FDG-PET studies. *J Nucl Med.* 1995;36:1714–1722.
8. Kudomi N, Bucci M, Oikonen V, et al. Extraction of input function from rat [^{18}F] FDG PET images. *Mol Imaging Biol.* 2011;13:1241–1249.
9. Fu Z, Tantawy MN, Peterson TE. Ensemble learning (EL) independent component analysis (ICA) approach to derive blood input function from FDG-PET images in small animal. *IEEE Nucl Sci Symposium Conf Record.* 2006;5:2708–2712.
10. Shoghi KI, Welch MJ. Hybrid image and blood sampling input function for quantification of small animal dynamic PET data. *Nucl Med Biol.* 2007;34:989–994.
11. Tantawy MN, Peterson TE. Simplified [^{18}F]FDG image-derived input function using the left ventricle, liver, and one venous blood sample. *Mol Imaging.* 2010;9:76–86.
12. Locke LW, Berr SS, Kundu BK. Image-derived input function from cardiac gated maximum a posteriori reconstructed PET images in mice. *Mol Imaging Biol.* 2011;13:342–347.
13. Naganawa M, Kimura Y, Ishii K, Oda K, Ishiwata K. Temporal and spatial blood information estimation using Bayesian ICA in dynamic cerebral positron emission tomography. *Digit Signal Process.* 2007;17:979–993.
14. Lei H, Berthet C, Hirt L, Gruetter R. Evolution of the neurochemical profile after transient focal cerebral ischemia in the mouse brain. *J Cereb Blood Flow Metab.* 2009;29:811–819.
15. Weber B, Burger C, Biro P, Buck A. A femoral arteriovenous shunt facilitates arterial whole blood sampling in animals. *Eur J Nucl Med Mol Imaging.* 2002;29:319–323.
16. Yu AS, Lin HD, Huang SC, Phelps ME, Wu HM. Quantification of cerebral glucose metabolic rate in mice using ^{18}F-FDG and small-animal PET. *J Nucl Med.* 2009;50:966–973.
17. Kehl MI. *Refinement and Standardization of Small Animal PET Scanning Experimentation and Data Analysis* [dissertation]. Zurich, Switzerland: ETH (Eidgenössische Technische Hochschule/Swiss Federal Institute of Technology); 2010.
18. Miskin JW. *Ensemble Learning for Independent Component Analysis* [dissertation]. Cambridge, U.K.: University of Cambridge; 2000.
19. Chugh BP, Lerch JP, Yu LX, et al. Measurement of cerebral blood volume in mouse brain regions using micro-computed tomography. *Neuroimage.* 2009;47:1312–1318.
20. Bland JM, Altman DG. Statistical methods for assessing agreement between two methods of clinical measurement. *Lancet.* 1986;1:307–310.
21. Pain F, Lanièce P, Mastrippolito R, Gervais P, Hantraye P, Besret L. Arterial input function measurement without blood sampling using a beta-microprobe in rats. *J Nucl Med.* 2004;45:1577–1582.
22. Green LA, Gambhir SS, Srinivasan A, et al. Noninvasive methods for quantitating blood time-activity curves from mouse PET images obtained with fluorine-18-fluorodeoxyglucose. *J Nucl Med.* 1998;39:729–734.
23. Wong KP, Sha W, Zhang X, Huang SC. Effects of administration route, dietary condition, and blood glucose level on kinetics and uptake of ^{18}F-FDG in mice. *J Nucl Med.* 2011;52:800–807.
24. Saha JK, Xia J, Grondin JM, Engle SK, Jakubowski JA. Acute hyperglycemia induced by ketamine/xylazine anesthesia in rats: mechanisms and implications for preclinical models. *Exp Biol Med (Maywood).* 2005;230:777–784.